International Journal of Engineering Sciences Paradigms and Researches (Volume 47, Issue: Special Issue of January 2018)
ISSN (Online): 2319-6564 and Website: www.ijesonline.com

One-pot template-free synthesis of heterophase $BiVO_4$ microspheres with enhanced photocatalytic activity

1.Mousumi Panda 2. B.N.Biswal
Nalanda Institute of Technology, Bhubaneswar
Dept. of Basic Science & Humanities
E-mail ID:mousumipanda@thenalanda.com

Abstract

The manufacture of $BiVO_4$ microspheres with tetragonal-monoclinic heterophase structures required the development of a one-pot, template-free hydrothermal technique. The development of the heterophase structure was confirmed by XRD and HRTEM characterizations. It was discovered that the hydrothermal time and molar ratio of Bi/V were crucial factors in the production of the heterophase structure and spherical morphology. In compared to pure monoclinic scheelite-type and tetragonal zircon-type $BiVO_4$, the as-prepared $BiVO_4$ microsphere demonstrated higher efficiency for RhB degradation thanks to its distinctive morphology and the presence of heterophase. The photoinduced active species were shown to be involved in the photocatalytic degradation of RhB by EPR and PL-TA methods. According to the electrochemical results, the improved photocatalytic activity is a result of the more efficient separation of photogenerated carriers produced in the heterophase $BiVO_4$ system.

Keywords: $BiVO_4$; Heterophase; RhB degradation; Photocatalytic degradation

1. Introduction

TiO_2-based heterogeneous photocatalysis has been intensively investigated for the elimination of a variety of toxic chemicals.[1-3] However, TiO_2 can only utilize the photons in the UV region due to its wide band gap (3.2 eV), which limits its possibility of employing visible light. To increase the photo-efficiency of TiO_2 under visible light, a great deal of attention is directed towards the modification of TiO_2 and the exploration of visible-light-driven photocatalysts.[4–7]

Bismuth vanadate ($BiVO_4$), as one of the most promising non-TiO_2 based photocatalysts, has been proven to have a good photocatalytic activity under visible light for organic molecule degradation such as rhodamine B (RhB) and also for O_2 evolution.[8] However, its practical applications are limited because of the poor electrical conductivity and the low separation efficiency of photogenerated electrons and holes.[9] As a result, a number of approaches have been developed to improve the photocatalytic activity of $BiVO_4$, including doping with metal/nonmetal atoms,[10,11] forming heterojunction structures,[12-15] reducing the size of $BiVO_4$ and controlling the morphology and phase structure of $BiVO_4$.[16-18] As we know, the photocatalytic activity of $BiVO_4$ is highly relevant to its crystal phase. $BiVO_4$ exists mainly in three crystalline phases: tetragonal scheelite, monoclinic scheelite and tetragonal zircon.[19] Among the three polymorphs, the tetragonal zircon-structured $BiVO_4$ (z-t $BiVO_4$) is least investigated and inactive compared with the comprehensively studied monoclinic scheelite $BiVO_4$ (s-m $BiVO_4$). Thus, one can tune $BiVO_4$ from inert to highly reactive, photocatalytic efficiency. For instance, it is well-known that commercially available Degussa P25 TiO_2 (80% anatase and 20% rutile) is widely used as a benchmark model photocatalyst due to its high activity. Researchers have found that the crystallized rutile layer growing on the surface of anatase greatly promotes the separation of photogenerated charge carriers. The work by Li et al. verified that the phase junction formed between the surface anatase nanoparticles and rutile particles could greatly enhance the photocatalytic activity for photocatalytic H_2 production.[20] Besides TiO_2-based materials, they also found that the tailored α–β phase junctions on the surface of Ga_2O_3 significantly enhanced the photocatalytic activity for water splitting.[21] And the transient absorption spectra further demonstrated the enhanced photocatalytic efficiency was ascribed to the efficient charge separation and transfer across the α–β phase junction.

Up to now, the search for such heterophase structured photocatalysts has focused mainly on UV light responsive catalysts.[22,23] Visible light active photocatalyst with heterophase structure has seldom been reported. He et al. prepared α-Fe_2O_3/γ-Fe_2O_3 heterophase nanorods by a facile thermal decomposition and redox method.[24] The material presented better visible-light photocatalytic performance than the single-phase α-Fe_2O_3 or γ-Fe_2O_3, suggesting that the well-structured interfaces and suitable band configuration were of great importance for enhancing its activity. More recently, Wang et al. found that a tight interface junction had been formed between $BiVO_4$ (s-m) and $BiVO_4$ (z-t) simply by means of controlling the phase composition. The formation of surface phase junctions has been demonstrated as an effective strategy for improving the

in a nanosize level.[25] Such a heterophase junction could promote electron migration across the interface, which accelerated the separation of photoinduced electron-hole pairs and obtained an increased photocatalytic activity. However, in the above studies, the heterophase materials were synthesized under relatively harsh conditions, such as high temperature, high pressure and multiple steps. Hence, a facile, energy-saving and environmental-friendly method was desirable for achieving the successful fabrication of heterophase semiconductor photocatalysts.

In the present paper, we developed a one-pot additive-free hydrothermal method to prepare $BiVO_4$ microsphere with z-t & s-m heterophase structure. The effect of hydrothermal temperature, holding time and Bi/V molar ratio in the starting materials were described in detail. The obtained samples were characterized by XRD, FESEM, HRTEM and UV-vis DRS. Subsequently, the photocatalytic activity of the sample was evaluated for the liquid-phase photocatalytic degradation of RhB under visible light irradiation ($\lambda > 420$ nm). To deeply understand the mechanism of heterophase system, special attention was paid to the investigation of the active species involved in the photocatalytic process. This work has scientific significance and gives a better understanding about the crystal phase of $BiVO_4$ and its role in the photocatalytic activity. Our studies would provide a possible strategy to develop highly active photocatalysts by designing and preparing the heterophase junctions.

2. Experimental section

Synthesis

All chemicals used were analytic grade reagents without further treatments. In a typical procedure, 0.02 mol of $Bi(NO_3)_3{\cdot}2H_2O$ was firstly dissolved into 20 mL of concentrated nitric acid with continuous stirring for 2 h. A certain amount of NH_4VO_3 with different Bi/V molar ratio was added to 20 mL of 6 M NaOH aqueous. Then, the NH_4VO_3 aqueous solution was added to the $Bi(NO_3)_3{\cdot}2H_2O$ solution to form a homogeneous mixture, which was subsequently dropped to the 30 mL of 6 M NaOH aqueous slowly. Plenty of colorful precipitation appeared immediately after the addition. The resulting precursor was stirred for 2 h and then transferred into a Teflon-lined stainless steel autoclave of 100 mL capacity. The autoclave was sealed and maintained at 180 ℃ for different holding time and then cooled down naturally. Finally, the products were collected by filtration, washed several times with deionized water and absolute alcohol, and dried at 60 ℃ for 8 h.

Characterizations

The X-ray diffraction (XRD) patterns of the synthesized catalysts were performed using a Bruker D8 Advance X-ray diffractometer at 40 kV and 40mA with Ni-filtered Cu Kα radiation. The morphology and particle size of the products were examined by field-emission scanning electron microscopy (FESEM) (Nova NanoSEM 230, FEI Corp.). High-resolution transmission electron microscopy (HRTEM) observation was carried out on a FEI Tecnai G2 F20 instrument operated at an accelerating voltage of 200 kV. The UV–vis diffuse reflectance spectra (DRS) were collected on a Varian Cary 500 spectrometer using $BaSO_4$ as a reference. N_2 adsorption-desorption measurements were conducted at 77 K on a Micrometritics ASAP2020 analyzer. Specific surface areas were determined by the Brunauer-Emmett-Teller (BET) method. Photoluminescence (PL) spectra were recorded on an Edinburgh FL/FS900 spectrophotometer. Electron paramagnetic resonance (EPR) signals were collected by a Bruker model A300 spectrometer (Bruker Instruments, Inc.) with the settings of center field (3512.48 G), microwave frequency (9.86 GHz), and power (6.35 mW). The photoelectrochemical experiment was measured using a CHI-660D electrochemical workstation filled with 0.1 M of Na_2SO_4 electrolyte (30 mL). The different $BiVO_4$ samples were deposited as a film form on a 5 mm × 5 mm ITO conductive glass that served as the working electrode. A Pt plate and an Ag/AgCl electrode were used as the counter electrode and reference electrode, respectively.

Tests of photocatalytic activity

RhB, a typical fluorone dye, was also selected as a model contaminant in the photocatalytic experiment. A 500 W halogen lamp (Philips Electronics) was used as illuminating source and placed in a cylindrical glass vessel in which cold water was circulating to avoid overheating. The system was cooled by using a fan to maintain at 25 °C. Two cutoff filters were equipped to completely remove any radiation below 420 nm, ensuring the $BiVO_4$/RhB aqueous mixture was irradiated only by visible light ($420 \text{ nm} < \lambda < 800$ nm). 0.08 g of photocatalyst was suspended in 80 mL of RhB aqueous solution (1×10^{-5} mol/L) and stirred for 2h in dark to ensure adsorption/desorption equilibrium had been reached. During irradiation, a 3 mL of the suspension was sampled at given time intervals, which was then centrifuged to remove the photocatalyst. A Varian Cary 50 Scan UV-vis spectrophotometer was used to record the concentration changes of the resulting degraded RhB solution. The percentage of degradation is reported as C/C_0. C is the absorption of RhB at each irradiated time interval of the maximum peak of the absorption spectrum at wavelength of 554 nm. And C_0 is the absorption of the initial concentration when adsorption/desorption equilibrium is achieved.

3. Results and discussion

Characterizations of catalysts

Fig. 1 shows the XRD patterns of the as-prepared samples as a function of hydrothermal reaction time and Bi/V molar ratios. When the Bi/V molar ratio was 4/1 and the synthesis temperature was 180 °C, the tetragonal zircon structure $BiVO_4$ (z-t $BiVO_4$, JCPDS No. 14-0133) was the dominant phase (Fig. 1a). As the reaction time increased to 48 h and 72 h, the peak at 28.8° for the monoclinic scheelite structure $BiVO_4$ (s-m $BiVO_4$, JCPDS No. 14-0688) appeared, indicating that the samples were mixture of z-t $BiVO_4$ and s-m $BiVO_4$ (z-t & s-m $BiVO_4$). Particularly, when the reaction time was 48 h, the sharp and narrow diffraction peaks indicated a high crystallinity of z-t $BiVO_4$. Thus, under the immobilization conditions (180 °C, 48 h), the influence of the Bi/V molar ratio on the phase structure of $BiVO_4$ was

investigated. As it can be seen in Fig. 1b, when the Bi/V molar ratio was 1/1 and 2/1, the XRD patterns of the samples were corresponding to the s-m $BiVO_4$. With the increasing of the Bi/V molar ratio, the z-t $BiVO_4$ was the dominant phase, and a small amount of s-m $BiVO_4$ was detected. The effect of reaction temperature on the phase compositions of $BiVO_4$ was also studied (Fig. S1 in Supplementary Information). When the reaction temperature was below 180 °C, the samples were in z-t $BiVO_4$ structure without any impurity phase. However, with further increase of reaction temperature up to 200 °C, all the z-t $BiVO_4$ transformed into the s-m $BiVO_4$. The XRD results indicated that lower Bi/V molar ratio, longer reaction time and higher temperature favored the formation of s-m $BiVO_4$. Moreover, the z-t & s-m heterophase $BiVO_4$ could be readily prepared by adjusting the Bi/V molar ratio and hydrothermal reaction time.

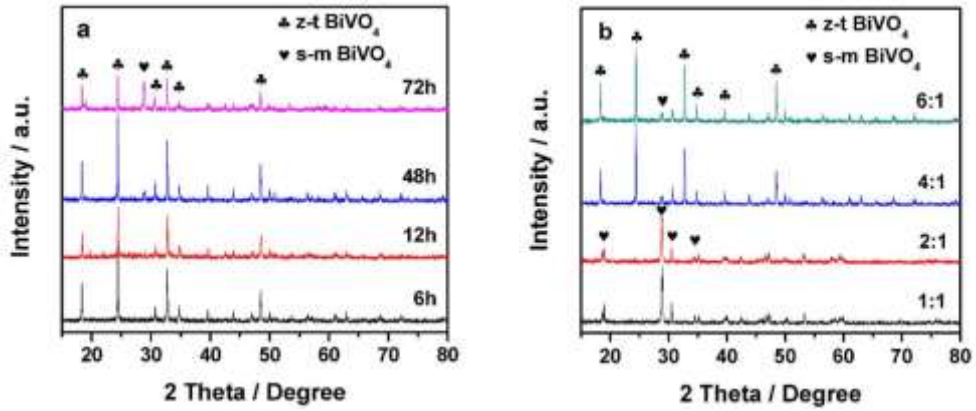

Fig.1 XRD patterns of $BiVO_4$ synthesized at 180 °C for different holding time with Bi/V molar ratio of 4/1 (a) and $BiVO_4$ synthesized at 180 °C for 48 h with different Bi/V molar ratios (b).

The morphologies of the as-prepared $BiVO_4$ samples were examined by FESEM technique. Fig. 2 presents FESEM images of the $BiVO_4$ samples with Bi/V molar ratio of 4/1 prepared at 180 °C for different holding time. When the reaction time was 6 h, relatively complete $BiVO_4$ microspheres with average diameters of about 3-5 μm formed (Fig. 2a), and the microspheres were composed of a large quantity of particles. As the reaction time extended to 12 h and 48 h, more and more microspheres collapsed, as shown in Fig. 2b and Fig. 2c. When the reaction time increased to 72 h, all the microspheres collapsed into irregular particles (Fig. 2d).

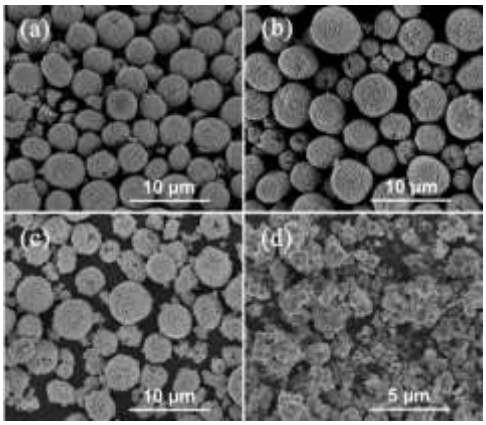

Fig.2 FESEM images of $BiVO_4$ samples with Bi/V molar ratio of 4/1 prepared at 180 °C for different holding time: (a) 6 h; (b) 12 h; (c) 48 h; (d) 72 h.

Fig. 3 shows the morphologies of as-synthesized $BiVO_4$ prepared at 180 °C for 48 h with different Bi/V molar ratios. When the Bi/V molar ratio were 1/1 and 2/1, the s-m $BiVO_4$ other (Fig. S2a). As the temperature increased to 200 °C, the spheres collapsed and lots of $BiVO_4$ particles formed (Fig. S2b). From these figures, we can come to a conclusion that the Bi/V molar ratio and hydrothermal time have significant effects on the morphologies of the samples. Fig. 4 shows the schematic illustration of various synthesis conditions and their corresponding structures.

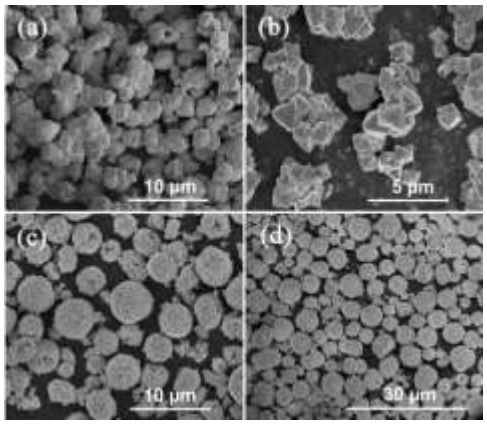

Fig.3 FESEM images of $BiVO_4$ samples prepared at 180 °C for 48 h with different Bi/V molar ratios: (a) 1/1; (b) 2/1; (c) 4/1; (d) 6/1.

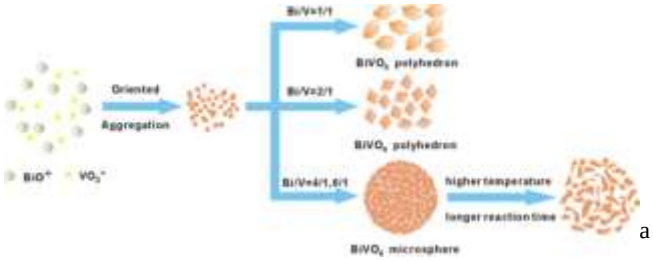

a size of ca. 1

μm, and the aggregation among particles was obvious (Fig. 3a, b). The products with Bi/V molar ratio of 4/1 and 6/1 were composed of a large quantity of microspheres with an average diameter of about 4-6 μm (Fig. 3c, d). The influence of hydrothermal temperature on the morphology was also investigated. When the product was treated at lower temperature, immature microspheres were observed which adhered with each

Fig.4 Schematic illustration of the synthesis conditions and their morphological results.

Fig. 5 shows the TEM images of the $BiVO_4$ sample prepared at 180 °C for 48 h with Bi/V molar ratio of 4/1. Part a of Fig. 5 presented an individual microsphere with a solid circle, in accordance with the corresponding FESEM image (Fig. 2c). Part b of Fig. 5 was the enlarged HRTEM image of the area marked by a red square in part a of Fig. 5. Obviously, two different kinds of lattice fringes were clearly presented. The distinct fringe of d = 0.467 nm matched that of the (011) crystallographic plane of s-m $BiVO_4$, while the fringe with interplanar spacing 0.258 nm was corresponding to (220) crystallographic plane of z-t $BiVO_4$. The above results further indicated that the as-synthesized sample was composed of z-t $BiVO_4$ and s-m $BiVO_4$, which was consistent with the results of XRD.

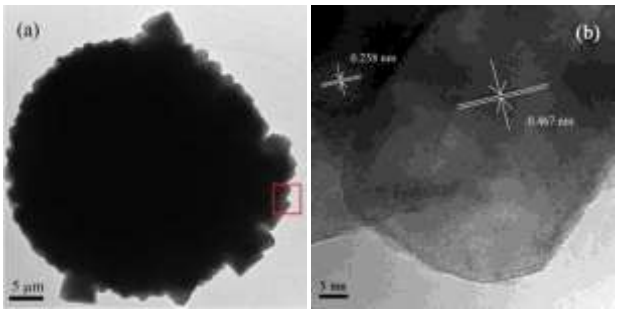

Fig.5 TEM and HRTEM images of $BiVO_4$ sample with Bi/V molar ratio of 4/1 prepared at 180 °C for 48 h.

Fig.6 displays the UV-vis DRS of the as-obtained $BiVO_4$ products. It can be seen that all the $BiVO_4$ products exhibited strong absorption in the visible range. From Fig. 6a, the light absorption exhibited red-shifts upon the increasing reaction time. As for the $BiVO_4$ sample synthesized for 6 h, the absorption intensity in the visible region was obviously lower than that of the other three samples, and the λ_{ab} ended at 429 nm with band gap of 2.89 eV. When the reaction time was 48 h, the λ_{ab} was estimated to be about 501 nm, corresponding to the band gap energy of 2.48 eV. With the reaction time increased to 72 h, the absorption intensity in the visible region was higher than that of the other samples. Varying the Bi/V molar ratio from 1/1 to 6/1, the light absorption exhibited blue-shifts (Fig. 6b). When the Bi/V molar ratio was 1/1, the XRD pattern was proved to be the s-m $BiVO_4$ phase. It showed the strongest visible-light-response among the four tested samples, and its absorption onset could be extended to 517 nm, corresponding to the band gap of 2.4 eV. When Bi/V molar ratio was 6/1, its absorption in the visible-light region was the weakest, corresponding to the highest band gap. The steep shape of the above two spectra indicates that their absorption in the visible-light region is due to the band gap transition.[26,27] Moreover, Fig. S3 shows that the light absorption exhibited red-shifts upon the increasing reaction temperature. When the treatment time was increased to 200 °C, the absorption onset dropped to 507 nm, corresponding to the band gap of 2.45 eV. The difference in the bandgaps of the as-prepared samples will make them show different photocatalytic activity under visible light irradiation.

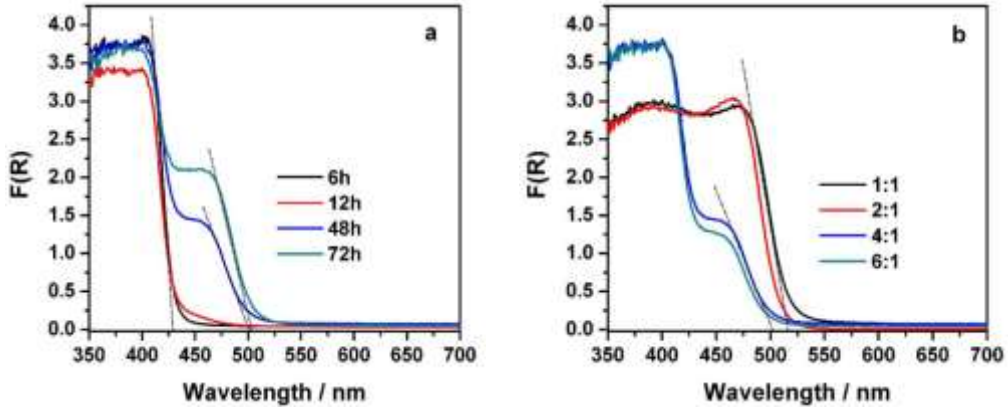

Fig.6 DRS of $BiVO_4$ samples with Bi/V molar ratio of 4/1 prepared at 180 °C for different holding time (a) and prepared at 180 °C for 48 h with different Bi/V molar ratios (b).

Photocatalytic degradation of RhB

The photocatalytic activities of the samples were mainly evaluated by measuring the photodegradation of RhB aqueous solution under visible light irradiation, as shown in Fig. 7. There was almost no decolorization in the solution without any catalysts. The absorption-desorption equilibrium was established after 2 h in dark absorption for $BiVO_4$ photocatalysts. After 6 h of irradiation time, the $BiVO_4$ sample prepared at 180 °C for 48 h exhibited the best activity, corresponding to the degradation ratio of about 97.7% after 6 h of visible light irradiation. It may result in the fact that when the reaction time was longer, the $BiVO_4$ microsphere collapsed and the formed $BiVO_4$ particles were

agglomerated and not well dispersed. Fig. 7b displays the concentration changes of RhB as a function of irradiation time in the presence of $BiVO_4$ samples prepared at 180 °C for 48 h with different Bi/V molar ratios. It is clear the RhB removal value over $BiVO_4$ with the Bi/V molar ratio of 1/1 was the lowest, and only 64.4% of RhB was decomposed after 6 h of visible light irradiation. On the contrary, the samples with the Bi/V molar ratio of 2/1 and 6/1 degraded 78.2% and 94.1% of RhB, respectively. In addition, the effect of hydrothermal temperature on the photocatalytic activity was also investigated (Fig. S4). The sample synthesized at different temperature exhibited different activities, and the catalyst prepared at 180 °C revealed the best activity. Based on the above results, the differences in the photocatalytic activity may be caused by the morphology and BET specific surface area of $BiVO_4$. The related information was summarized as shown in Table 1. According to $V_{monoclinic} = I_{monoclinic(121)} / (I_{monoclinic(121)} + I_{tetragonal(200)})$,[28] the percentage of the monoclinic phase was calculated.

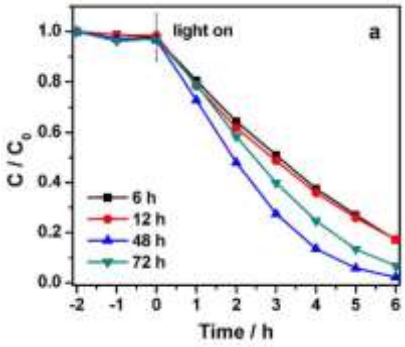

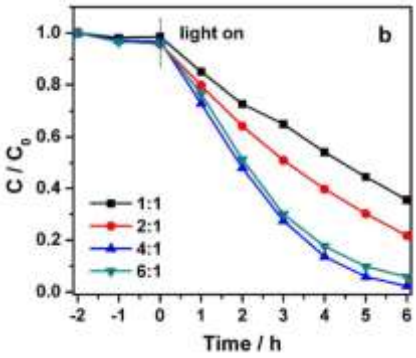

Fig.7 Degradation curves of RhB over the $BiVO_4$ samples with Bi/V molar ratio of 4:1 prepared at 180 °C for holding different time (a), prepared at 180 °C for 48 h with different Bi/V molar ratios (b).

Table 1 Crystal structures and RhB degradation ratio of $BiVO_4$ samples obtained under different preparation conditions.

Bi/V	Temperature (°C)	Time (h)	mon./(mon.+tetr.)[a]	BET surface area ($m^2 \cdot g^{-1}$)	RhB degradation ratio (%)
4/1[b]	180	6	0	2.42	82.9
4/1	180	12	0	2.02	82.7
1/1[c]	180	48	1	0.57	64.4
2/1	180	48	1	0.87	78.2
4/1[d]	180	48	0.1	2.62	97.7
4/1	120	48	0.06	1.63	67.6
4/1	200	48	1	0.94	84.7
6/1	180	48	0.11	2.58	94.1
4/1	180	72	0.44	1.04	93.1

[a] mon./(mon.+tetr.) denotes the percentage of the monoclinic phase in the heterophase. [b] The $BiVO_4$ sample is abbreviated as z-t $BiVO_4$. [c] The $BiVO_4$ sample is abbreviated as s-m $BiVO_4$. [d] The $BiVO_4$ sample is abbreviated as z-t & s-m $BiVO_4$.

Photocatalytic activity discussions

To clarify the reasons of the enhanced photocatalytic activity, we detected the involved active species forming in the photocatalytic reaction under visible light irradiation. In order to simplify the experiment, the above three $BiVO_4$ samples (b, c, d in Table 1) were selected as models for the further study. To recognize the formation of hydroxyl radicals (•OH), the TA-PL probing technique was firstly used in the $BiVO_4$ systems.[29] In the $BiVO_4$/TA system, when irradiated with visible light, 2-hydroxyl-terephthalic acid is generated, which is captured by terephthalic acid (TA) and performs a strong fluorescence characteristic (Fig. 8). So monitoring the fluorescence intensity changes of 2-hydroxyl-terephthalic acid in $BiVO_4$/TA suspension, we can indirectly detect the generation of hydroxyl radicals. Fig.8 shows the •OH-trapping PL spectra of suspensions containing different photocatalysts and TA. As we can see, the fluorescence intensity increased in different degrees with the irradiation time within 6 h. It can be concluded that hydroxyl radicals were indeed generated in the $BiVO_4$ suspension under visible light irradiation. The z-t & s-m $BiVO_4$ which presented the best photocatalytic activity generated the most hydroxyl radicals. And the general trend of hydroxyl radical generation was in accordance with that of RhB degradation, suggesting hydroxyl radical were indeed generated on $BiVO_4$ under visible light irradiation as one of the active species.

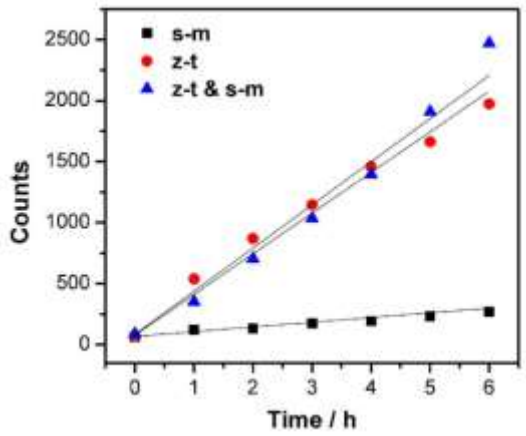

Fig.8 The comparison plot of temporal changes in •OH-trapping PL spectra of s-m $BiVO_4$, z-t $BiVO_4$ and z-t & s-m $BiVO_4$ under visible light irradiation.

The spin trapping EPR technique was also used to detect the reactive oxygen species generated in the heterophase photocatalytic process. Fig.9 shows the spin-trapping EPR spectra of z-t & s-m $BiVO_4$. It could be seen that there was no obvious signal corresponding to DMPO–•OH and DMPO–O_2•$^-$ in dark. However, under visible light irradiation, four characteristic peaks of DMPO–•OH could be obviously observed in the suspension. Similarly, only under visible light irradiation, the six characteristic peaks corresponding to the spin-adducts DMPO–O_2•$^-$ could be observed in the methanol solvent. On the basis of the above characterization, it indicated that •OH and O_2• species existed and participated in the degradation process.

subsequent decomposition. Another is the presence of AO aborted the generation of active species and high mobility of charge carriers of the circulatory system which seriously inhibits the photocatalytic degradation process. Tert-butyl alcohol (TBA), as a scavenger for •OH, was also added in the system. From the figure, in the presence of 2 mL of TBA, the degradation ratio of RhB was decreased to 88% after 6 h of irradiation. So, the RhB oxidation was driven by the contribution of •OH radicals to a lesser extent. It is worth noting that the condition after adding the benzoquinone (BQ) was quite different. BQ has the ability to trap O_2•$^-$ by a simple electron transfer mechanism.[33,34] With the addition of 1 mg of BQ, the rate for degradation of RhB over z-t & s-m $BiVO_4$ was dramatically decreased and only about 15% of RhB was degraded.

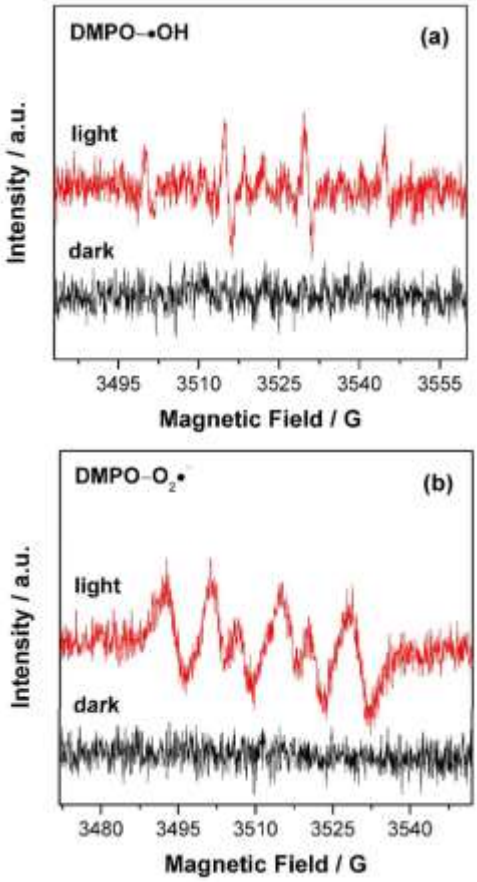

Fig.9 EI rsion for DMPO– (420 nm

To further evaluate the role of these active species such as electrons/holes, •OH and O_2•$^-$, some additional conditions that affected the generation of active species were applied in the degradation process.[30,31] Fig. 10 shows the photocatalytic activity of z-t & s-m $BiVO_4$ towards the degradation of RhB under different conditions. Without the addition of the scavengers, the photocatalytic degradation rate of RhB is 97.7% after 6 h of visible irradiation (the original curve). Ammonium oxalate (AO) is an effective scavenger of holes.[32] After 0.1 g of AO was added to the reaction system, the degradation ratio of RhB was decreased to 75%. The addition of AO inhibited the photocatalytic degradation process. There are two reasons: one is that the photogenerated hole in heterophase $BiVO_4$ would activate some unsaturated organic pollutants, resulting in

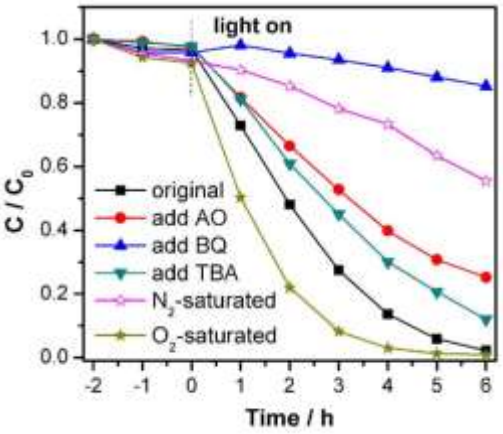

Fig.1 nder differ g AO,

Moreover, dissolved O_2 as an efficient electron scavenger and an important source of O_2• was excluded under flowing N_2 gas (flow rate: 50 mL·min^{-1}) in the degradation process. After the light irradiation, the photocatalytic conversion ratio was decreased to 44%. And by bubbling O_2 gas (flow rate: 50 mL·min^{-1}), the dissolved O_2 could be increased and the corresponding degradation ratio was increased. Therefore, the electrons or the active species generated by electrons play an important role in the heterophase photocatalytic reaction. A combination of the results of EPR and the addition of BQ indicates that O_2•$^-$ played a very important role in the photocatalytic process. And the holes and •OH were the subordinate factors. However, we can still detect the signal of •OH on the surface of heterophase $BiVO_4$ by TA-PL and EPR techniques. To sum up, through the comparison, we can conclude that the RhB oxidation was driven mainly by the participation of O_2•$^-$ and holes, and to a lesser extent by the contribution of •OH. In addition, photoelectrochemical technique was applied to study the charge transfer and separation of photogenerated electron-hole pairs over the photocatalyst/electrolyte interfaces. The photocurrent density-time (I-t) profiles without any bias electrode potential were given as shown in Fig. 11a. When visible light source was turned on or off, the instantaneous photocurrent of pure s-m $BiVO_4$ and z-t $BiVO_4$ were in a small degree, which was corresponding to the weak photodegradation of organic pollutants. The photocurrent resulted from the photogenerated electron/hole pairs of excited $BiVO_4$ under visible light irradiation. Obviously, the photocurrent of z-t & s-m $BiVO_4$ was greatly increased at given time intervals (40 s). Furthermore, electrochemical impedance spectroscopy (EIS) was also used to investigate the charge transfer resistance and the separation efficiency of photogenerated charge. Fig. 11b shows EIS response of s-m/z-t $BiVO_4$/FTO films and z-t & s-m $BiVO_4$/FTO film under visible-light irradiation. The radius of the arc on the EIS Nynquist plot reflects the reaction rate occurring at the surface of electrode. Obviously, the arc radius on EIS Nynquist plot of z-t & s-m $BiVO_4$/FTO film was smaller than that of z-t $BiVO_4$/FTO film and s-m $BiVO_4$/FTO film samples. It indicates that z-t & s-m $BiVO_4$ has lower resistance than that of pure s-m $BiVO_4$ and z-t $BiVO_4$. The results of photoelectrochemical tests

indicated that the presence of heterophase was capable of improving separation efficiency and effectively inhibit the electron-hole pair recombination. Thus, the z-t & s-m heterophase $BiVO_4$ had a higher photocatalytic performance compared with the pure s-m $BiVO_4$ and z-t $BiVO_4$. In conclusion, the RhB oxidation over z-t & s-m heterophase $BiVO_4$ was driven mainly by the participation of electrons and $O_2^{\bullet-}$ radicals, and to a lesser extent by the contributions of holes and •OH radicals. These radicals attacked the RhB molecules adsorbed on the surface of catalyst, leading to the efficiently photocatalytic oxidation of RhB. Our studies open a door toward facile improvement in the efficiency of $BiVO_4$, promoting its great potential in environmental pollutant cleanup applications.

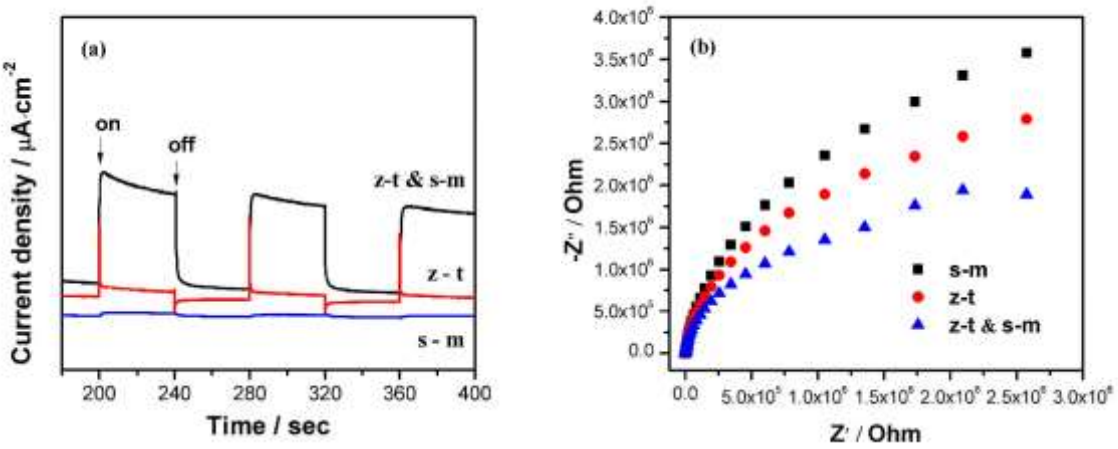

Fig.11 (a) Comparison of transient photocurrent responses and (b) EIS Nynquist plots of the s-m $BiVO_4$, z-t $BiVO_4$ and z-t & s-m $BiVO_4$ under visible light irradiation (420 nm < λ < 800 nm, $[Na_2SO_4]$ = 0.1 M).

4. Conclusions

In summary, $BiVO_4$ microsphere with tetragonal-zircon/monoclinic-scheelite heterophase, had been successfully synthesized via a one-pot template-free hydrothermal method. The formation of heterophase had a significant influence on the microstructures and photodegradation efficiency of the photocatalyst. Benefiting from the high surface area and extended absorption in the visible light region, the heterophase $BiVO_4$ sample exhibited the highest photocatalytic activity with 97.7% of RhB degraded, remarkably superior to the pure monoclinic-scheelite $BiVO_4$ and tetragonal-zircon $BiVO_4$. Such an improved photocatalytic activity was ascribed to the most effectively separation efficiency of photogenerated carriers generated in the heterophase $BiVO_4$ system, as evidenced by the electrochemical measurement. •OH and $O_2^{\bullet-}$ had been detected in the suspension of heterophase $BiVO_4$ microsphere by the TA-PL and EPR techniques. Based on free-radical scavenging and N_2/O_2 purging experiments, the decomposition of RhB was driven mainly by the participation of $O_2^{\bullet-}$ and a lesser extent by the participation of holes and •OH.

Acknowledgements

The authors gratefully acknowledge financial support for this research from the National Natural Science Foundation of China (21173047, 21373049 and 31260400), the Natural Science Foundation of Jiangxi (20142BAB213012, 20122BAB214003), Science and Technology Support Project of Jiangxi (20142BBE50007), Scientific Research Foundation of Jiangxi Academy of Sciences, and Open Project from State Key Laboratory of Photocatalysis on Energy and Environment of Fuzhou University.

Notes and references

[a]*Research Institute of Applied Chemistry, Jiangxi Academy of Sciences, Nanchang, Jiangxi, 330096, P. R. China.*
[b]*Research Institute of Photocatalysis, State Key Laboratory of Photocatalysis on Energy and Environment, Fuzhou University, Fuzhou, 350002, P. R. China. Fax: +86-591-83779256; Tel: +86-591-83779256; E-mail: dzli@fzu.edu.cn.*

1 M. R. Hoffmann, S. T. Martin, W. Y. Choi and D. W. Bahnemann, *Chem. Rev.*, 1995, **95**, 69.
2 C. C. Chen, W. H. Ma and J. C. Zhao, *Chem. Soc. Rev.*, 2010, **39**, 4206.
3 H. H. Chen, C. E. Nanayakkara and V. H. Grassian, *Chem. Rev.*, 2012, **112**, 5919.
4 M. Nolan, *Chem. Commun.*, 2011, **47**, 8617.
5 W. J. Zhou, Z. Y. Yin, Y. P. Du, X. Huang, Z. Y. Zeng, Z. X. Fan, H. Liu, J. Y. Wang and H. Zhang, *Small*, 2013, **9**, 140.
6 Z. G. Yi, J. H. Ye, N. Kikugawa, T. Kako, S. X. Ouyang, H. Stuart Williams, H. Yang, J. Y. Cao, W. J. Luo, Z. S. Li, Y. Liu and R. L. Withers, *Nat. Mater.*, 2010, **9**, 559.
7 Y. H. He, D. Z. Li, J. Chen, Y. Shao, J. J. Xian, X. Z. Zheng and P. Wang, *RSC Adv.*, 2014, **4**, 1266.

8 A. Kudo, K. Omori and H. Kato, *J. Am. Chem. Soc.*, 1999, **121**, 11459.
9 Y. Park, K. J. McDonald and K. S. Choi, *Chem. Soc. Rev.*, 2013, **42**, 2321.
10 C. Yin, S. M. Zhu, Z. X. Chen, W. Zhang, J. J. Gu and D. Zhang, *J. Mater. Chem. A*, 2013, **1**, 8367.
11 X. F. Zhang, Y. B. Zhang, X. Quan and S. Chen, *J. Hazard. Mater.*, 2009, **167**, 911.
12 M. C. Long, W. M. Cai, J. Cai, B. X. Zhou, X. Y. Chai and Y. H. Wu, *J. Phys. Chem. B*, 2006, **110**, 20211.
13 Y. Hu, D. Z. Li, Y. Zheng, W. Chen, Y. H. He, Y. Shao, X. Z. Fu and G. C. Xiao, *Appl. Catal. B: Environ.*, 2011, **104**, 30.
14 Z. Q. He, Y. Q. Shi, C. Gao, L. N. Wen, J. M. Chen and S. Song, *J. Phys. Chem. C*, 2014, **118**, 389.
15 M. D. Han, T. Sun, P. Y. Tan, X. F. Chen and O. K. Tan, *RSC Adv.*, 2013, **3**, 24964.
16 W. D. Shi, Y. Yan and X. Yan, *Chem. Eng. J.*, 2013, **215**, 740.
17 G. C. Xi and J. H. Ye, *Chem. Commun.*, 2010, **46**, 1893.
18 R. G. Li, F. X. Zhang, D. E. Wang, J. X. Yang, M. R. Li, J. Zhu, X. Zhou, H. X. Han and C. Li, Nat. Commu. 2013, **4**, 1432.
19 S. Tokunaga, H. Kato and A. Kudo, *Chem. Mater.*, 2001, **13**, 4624.
20 J. Zhang, Q. Xu, Z.C. Feng, M. J. Li and C. Li, *Angew. Chem. Int. Ed.*, 2008, **47**, 1766.
21 X. Wang, Q. Xu, M. R. Li, S. Shen, X. L. Wang, Y. C. Wang, Z. C. Feng, J. Y. Shi, H. X. Han and C. Li, *Angew. Chem. Int. Ed.*, 2012, **51**, 13089.
22 K. Pan, Y. Z. Dong, W. Zhou, G. F. Wang, Q. J. Pan, Y. Yuan, X. H. Miao and G. H. Tian, *Electrochim. Acta*, 2013, **88**, 263.
23 Y. X. Liu, Z. L. Wang, W. D. Wang and W. X. Huang, *J. Catal.*, 2014, **310**, 16.
24 Z. W. Wei, X. C. Wei, S. Y. Wang and D. Y. He, *Mater. Lett.*, 2014, **118**, 107.
25 H. M. Fan, T. F. Jiang, H. Y. Li, D. J. Wang, L. L. Wang, J. L. Zhai, D. Q. He, P. Wang and T. F. Xie, *J. Phys. Chem. C*, 2012, **116**, 2425.
26 A. P. Zhang, J. Z. Zhang, N. Y. Cui, X. Y. Tie, Y. W. An and L. J. Li, *J. Mol. Catal. A: Chem.*, 2009, **304**, 28-32.
27 Y. N. Guo, X. Yang, F. Y. Ma, K. X. Li, L. Xu, X. Yuan and Y. H. Guo, *Appl. Surf. Sci.*, 2010, **256**, 2215-2222.
28 A. K. Bhattacharya, K. K. Mallick and A. Hartridge, *Mater. Lett.*, 1997, **30**, 7.
29 J. C. Barreto, G. S. Smith, N. H. P. Strobel, P. A. Mcquillin and T. A. Miller, *Life Sci.*, 1995, **56**, 89.
30 W. J. Li, D. Z. Li, Y. M. Lin, P. X. Wang, W. Chen, X. Z. Fu and Y. Shao, *J. Phys. Chem. C*, 2012, **116**, 3552.
31 W. J. Li, D. Z. Li, J. X. Wang, Y. Shao, J. M. You and F. Teng, *J. Mol. Catal. A: Chem.*, 2013, **380**, 10.
32 H. Kominami, A. Furusho, S. Murakami, H. Inoue, Y. Kera and B. Ohtani, *Catal. Lett.*, 2001, **76**, 31.
33 M. Stylidi, D. I. Kondarides and X. E. Verykios, *Appl. Catal. B: Environ.*, 2004, **47**, 189.
34 P. Raja, A. Bozzi, H. Mansilla, J. Kiwi, *J. Photochem. Photobiol. A*, 2005, **169**, 271.